Full Paper can be found for free until November 28, 2017 here

https://authors.elsevier.com/a/1VsDR1M7w0FFRz

Afterwards full paper is found here:

http://www.sciencedirect.com/science/article/pii/S0378775317313277

Title: Post-Mortem Analysis on LiFePO<sub>4</sub>|Graphite cells describing the evolution & composition of covering layer on anode and their impact on cell performance

## **Authors**

Meinert Lewerenz<sup>a,b</sup>, Alexander Warnecke<sup>a,b</sup>, Dirk Uwe Sauer<sup>a,b,c</sup>

## **Affiliation**

- a) Electrochemical Energy Conversion and Storage Systems Group, Institute for Power Electronics and Electrical Drives (ISEA), RWTH Aachen University, Jägerstrasse 17/19, D-52066 Aachen, Germany
- b) Juelich Aachen Research Alliance, JARA-Energy, Germany
- c) Helmholtz Institute Münster (HI MS), IEK-12, Forschungszentrum Jülich, Corrensstrasse 46, 48149 Münster, Germany

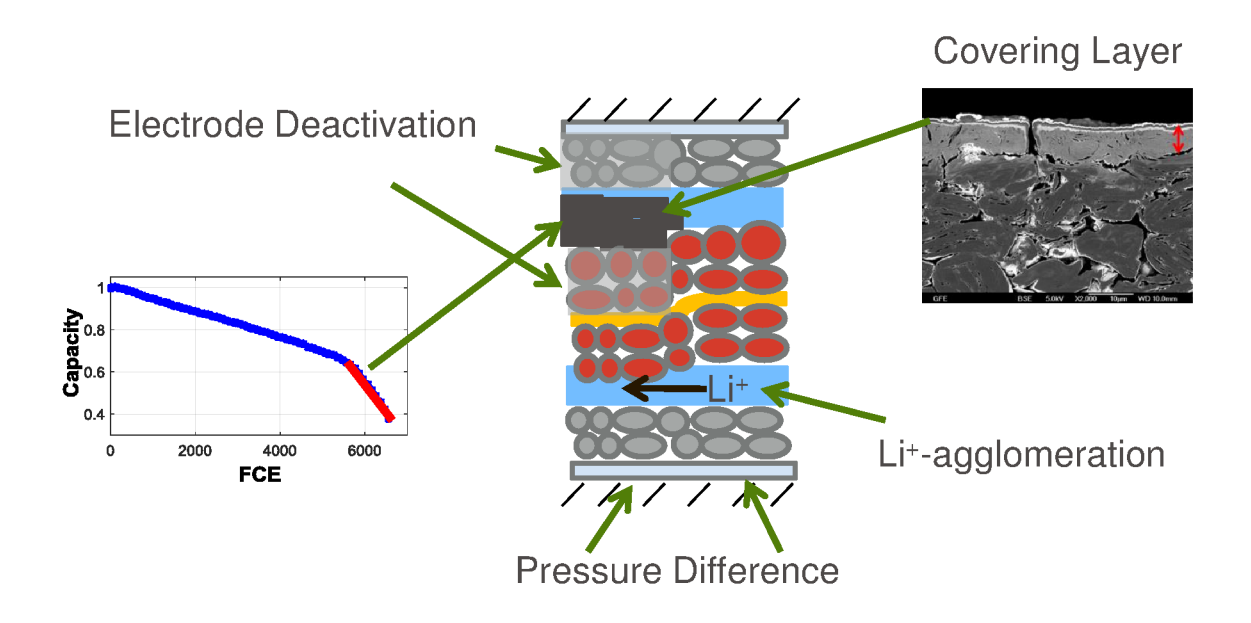
## Abstract

During cyclic aging of lithium-ion batteries the formation of a  $\mu$ m-thick covering layer on top of the anode facing the separator is found on top of the anode. In this work several post-mortem analyses of cyclic aged cylindrical LFP|Graphite cells are evaluated to give a detailed characterization of the covering layer and to find possible causes for the evolution of

such a layer. The analyses of the layer with different methods return that it consists to high percentage of plated active lithium, deposited Fe and products of a solid electrolyte interphase (SEI). The deposition is located mainly in the center of the cell symmetrical to the coating direction. The origin of these depositions is assumed in locally overcharged particles, Fe deposition or inhomogeneous distribution of capacity density. As a secondary effect the deposition on one side increases the thickness locally; thereafter a pressure-induced overcharging due to charge agglomeration of the back side of the anode occurs. Finally a compact and dense covering layer in a late state of aging leads to deactivation of the covered parts of the anode and cathode due to suppressed lithium-ion conductivity. This leads to increasing slope of capacity fade and increase of internal resistance.

# **Key Words**

Cyclic aging, post-mortem analysis, covering layer, electrode deactivation, plating



## **Abbreviations**

FCE: full cycle equivalents

DVA: differential voltage analysis

CDA: capacity difference analysis

PMA: Post-mortem-analysis

EC: ethylene carbonate

DMC: dimethylene carbonate

EMC: ethylene-methylene carbonate

DEC: diethylene carbonate

LFP: lithiumironphosphate

SEI: solid electrolyte interphase

DOD: depth-of-discharge

SOC: state-of-charge

EIS: electrochemical impedance spectroscopy

HF: hydrofluoric acid

CMC: carboxymethyl cellulose

SBR: styrene-butadiene rubber

PVDF: polyvinylidene fluoride

# 1. Introduction

This contribution summarizes the findings of the cell tests on 50 cylindrical 8 Ah LFP|Graphite and additional post-mortem analyses (PMA) to describe the evolution and the influence of a dense covering layer on top of the anode facing the separator. The dense covering layer is found exclusively for cells aged in cycle tests. Therefore, the covering layer cannot be described solely by calendaric aging effects as reported e.g. by Kassem et al. [1].

The degradation of the cells is analyzed with different methods. In [2] the trends of capacity and internal resistance for these cells are discussed. The covering layer was only found for cyclic aged cells but not for calendaric aged cells [3] which is in good accordance to literature [4–6]. The covering layer on top of the anode facing the separator is reported for the following cathode materials: LiFePO4<sub>4</sub> [2,4,5] and LiMn<sub>2</sub>O<sub>4</sub>/Li(Ni<sub>0.5</sub>Co<sub>0.2</sub>Mn<sub>0.3</sub>)O<sub>2</sub> [6].

The covering layer of the discussed cells was not found for all test conditions and equally tested cells did not necessarily show the same deposition pattern [3]. Therefore, the deposition is assumed to be most likely additionally influenced by the homogeneity of the coating in form of bad contacted particles or inhomogeneous distribution of capacity density. This conclusion is supported by the fact that the deposition was always found in direction of winding or coating at the center or the edges of the electrode's height, respectively [2,3]. Other constraints that are related to the winding direction are temperature and pressure. Those two parameters are further increasing towards the cell's center due to increasing friction and higher distance to the colder housing. This becomes crucial especially for cycling at high C-rates.

Strong inhomogeneities induced e.g. by the evolution of covering layer are detectable with the capacity difference analysis (CDA) which is a non-destructive method to evaluate the difference of capacities measured at 1C and 0.25C [3]. If the capacity difference shows a strong rise during aging, the evolution of a covering layer is associated. This is supported by evaluating the differential voltage analysis (DVA) as it is shown in [7]. Here increasing

inhomogeneity and loss of anode active material could be associated to the evolution of a covering layer. Furthermore, there are publications that found a correlation between the formation of covering layer with the increase of impedance and loss of active lithium [4,6].

The morphology of the deposition is depending on core temperature of the cell, the applied C-rate and the voltage regime of the cycling [3]. There seems not to be an intuitive and simple C-rate dependency, as the cycling at higher C-rates of 4C and 8C did not lead to a dense covering layer whereas for 1C and 2C partially a covering layer could be observed. Since the C-rate gets along with resistive heat, the temperature might play a key role, too. An interesting finding is that the 1C cycling with the lowest DOD between 45-55% SOC at 40 °C leads to strong formation of covering layer, although the charge cut-off voltage is far away reducing risk of plating and nearly no volume expansion that may affect active material is expected. The evaluation of DVA leads to the assumption that due to the flat voltage curves of anode and cathode cycling induced inhomogeneous distribution of active lithium is not compensated under these test conditions. Thus, during the following check-up plating is likely [7].

The covering layer is discussed as a solid-electrolyte interphase (SEI) or something that is in conjunction with passivated lithium plating. This is assumed as it is not found surrounding the graphite particle, which would be expected for calendaric aged cells. According to Klett et al. [5] for LiFePO<sub>4</sub>|Graphite the covering layer is rich in P-O bonds and contains Fe and carbonate species. Finally according to Klett et al. [5] the residual composition is similar to the SEI of a calendaric aged cell.

In this contribution the formation of covering layer is discussed on behalf of three aged cells. Therefore, the morphology, the chemistry and the electro-chemistry are examined and linked to the full cell test results. Special focus is put on the causes leading to covering layer evolution on the primary and on the secondary side of the double-coated anode. The primary side is defined as the side where the covering layer evolution initially takes place. Finally the theory of deactivation of anode and cathode due to an impermeable covering layer will be

proved by too high amount of lithium on the cathode and by geometrical approach considering the deactivated electrode area to explain the superposed capacity loss and internal resistance increase.

# 2. Experimental

# 2.1 Cell, Aging and Check-ups

The detailed description of the cells and the aging is already given in [2] and only a short excerpt is given here.

The tested cell is a cylindrical 8 Ah cells with LiFePO<sub>4</sub> (LFP) on the cathode, graphite on the anode and (EC-DMC-DEC-EMC)-LiPF<sub>6</sub> as electrolyte. The tests are performed at 40 °C temperature of the cell's case in a temperature chamber. The DODs of partial cycles are related to the nominal capacity. After a complete charge the mean SOC of 50% of the corresponding cycle, defined using the current capacity, was approached Ah-based. This is necessary as approaching voltage–based is difficult since LiFePO<sub>4</sub> is featured by a very flat open circuit voltage (OCV) curve.

Three aged cells were tested under the following conditions: 1C 45-55% SOC, 1C 0-100% SOC and 2C 25-75% SOC. After end of test a covering layer was observed in all three cells by using PMA.

The check-ups are performed at a chamber temperature of 25 °C between 2.0 V to 3.65 V. The capacity is measured at 1C and a low current cycle is performed at 0.25C used for CDA and DVA. Additionally, a 10 s-discharge-pulse at 50% SOC is evaluated.

# 2.2 Post-Mortem Analysis

The post-mortem analyses are performed under argon atmosphere in a fully discharged or fully charged state. The cells are evaluated by their surface morphology and color using a Keyence VK-9710 laser microscope (confocal microscope).

Scanning electron microscopy (SEM) results were obtained on a JEOL JEM-7001F, with an EDX detector from EDAX. The SEM was mainly used at a low energy (5 kV), in order to increase the surface sensitivity. Images presented here are both using secondary electrons and backscattered electrons depending on what should be emphasized.

The samples were prepared for SEM using a cross-section polisher (JEOL) applying a broad Argon ion beam to cut through the material and give a very smooth surface without having to get the sample into contact with water or traditional polishing abrasives. The cross-section polisher was run at 4 kV for the graphite anodes and 6 kV for the cathodes, for up to 6 hours. The samples were exposed to air up to one minute before placed in the cross-section polisher, and up to thirty seconds of air during transportation from the cross-section polisher to the SEM.

To measure the electrode thickness a micrometer screw Micromar 40 E was used with a precision of 2  $\mu$ m and a scale-reading precision of 1  $\mu$ m.

The lithium distribution is measured with Varian ICP-OES (inductively coupled plasma-optical emission spectrometer), shortened to ICP. Therefore 15 spatial distributed 20 mm-diameter-discs of the double-coated electrodes are taken. As preparation each sample was washed with DMC before it is dissolved in agua regia.

For half-cell tests one electrode side was removed with methanol for the anode (CMC/SBR binder) and NMP (N-Methyl-2-pyrrolidon) for the cathode (PVDF binder). 15 samples per electrode of a diameter of 16 mm are mounted in a coin cell vs. lithium metal, respectively. To obtain a trend over electrode length samples are harvested at the inner part, in middle part and at end part of the electrode's length respectively. A trend over the electrode's height is achieved by evaluating five distributed samples over electrode's height at all three positions of length. As a separator Whatman GF-C was used. The check-up capacities are evaluated at C-rate of 0.1C for the anode in the window of 5 mV to 2.0 V and for the cathode in the window of 1.8 V to 3.8 V. The cells are cycled using a BaSyTec CTS system.

# 3. Results and Discussion

The evolution of covering layer deposition and their impact on cell performance is demonstrated exemplarily for two fresh cells and three aged cells. Two of the aged cells are discussed in depth and therefore shortened to 1C-cell (1C 0-100% SOC) and 2C-cell (2C 25-75% SOC).

Table 1 The material capacities of spatial resolved half-cell tests graphite vs. lithium. The harvested samples have a diamter of 16 mm. Displayed are averaged values at several positions of the fresh cell, 2C-cell and the 1C –cell.

	Fresh cell	2C-cell	1C-cell
	$\text{mAh}\cdot\text{cm}^{-2}$	$\text{mAh}\cdot\text{cm}^{-2}$	$\text{mAh}\cdot\text{cm}^{-2}$
Cathode	6.15	6.41	6.31
Anode (center)	2.24	6.94	6.29
Anode (top/bottom)	6.94	7.54	6.65

# 3.1 Inhomogeneous charged anode

The origin of the here discussed thick covering layer on top of the anode facing the separator are originated from inhomogeneities in the cells that will lead to a local overcharge of the anode. This should be separated from classically provoked lithium plating by combining high charging currents up to the cut-off voltage with low temperatures in the order of 0 °C or lower. In this case rather homogeneous plating over the anode combined with a high loss of active lithium within one charge process is expected. A high portion of this lithium deposition will be reversible plating that can be reactivated during the following discharge. This is nicely shown by Lu et al. [8] and Petzl et al. [9]. In this contribution the discussed thick passivated covering layer is observed after a long period of aging of partially more than 5,000 FCE at 40 °C and for the high power cell moderate C-rates and for some test conditions far away from the cut-off voltage.

## Coating inhomogeneity (2C-cell)

A simple cause for inhomogeneities is an uneven distribution of active material within the coating or a bad cell balancing where the cathode's capacity is greater than the anode's capacity. Several half-cell measurements of a fresh cell exhibit a typical capacity density of the coating of 6.15 mAh · cm<sup>-2</sup> for the cathode and 6.94 mAh · cm<sup>-2</sup> for the anode (Table 1). In the case of the 2C-cell the anode reveals a normal capacity of 6.94 mAh · cm<sup>-2</sup> in the center and a smoothly increasing capacity up to 7.54 mAh · cm<sup>-2</sup> at the edges. The DVA gives no evidence for continuous loss of anode capacity but for deactivation of parts of the anode [7]. Due to fracturing of the covering layer during disassembling the layer becomes permeable again. Therefore, the half-cell capacities measured at 0.1C are assumed to be comparable to those measured at begin of test.

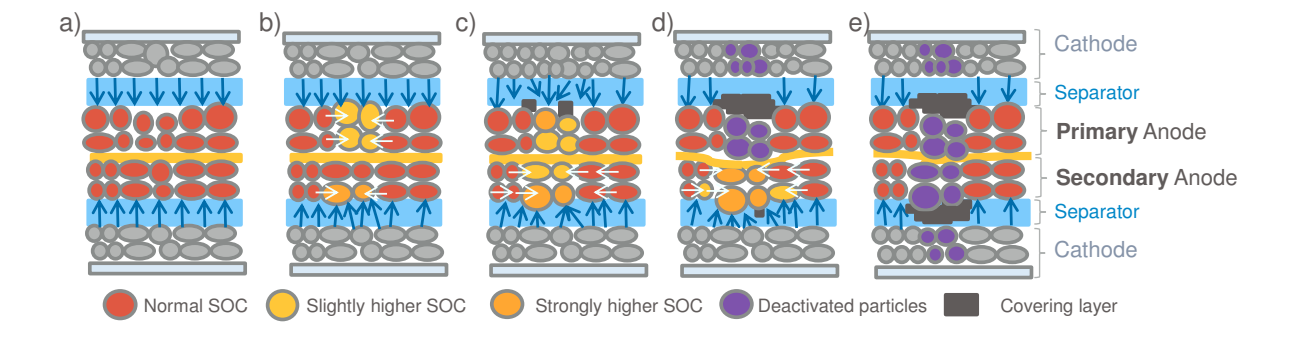


Figure 1 Schematic of the covering layer evolution on the primary and the secondary anode side (back side) for a cell with inhomogeneous coating. The primary side is defined where the covering layer takes place first. The covering layer is sketched in black. Charge agglomeration is highlighted from yellow to orange. Purple particles are deactivated. Arrows represent the lithium-ion flow between anode and cathode (blue) and within the anode (white).

An uneven capacity density over the anode is already problematic during the formation process since the SEI will be formed with different quality at different regions of the anode. With this, locally higher aging and overcharging of special regions might build the basis for the evolution of a dense covering layer. A schematic for primary side, where the covering layer evolution takes place at first, is shown in the top part of Figure 1 a)-d). The initially

homogeneous charge currents in a) resulting in higher SOC in the center part with lower capacity density in b) until finally overcharging and plating lead to covering layer evolution.

The first deposition on top of the anode (primary side) in Figure 1c induces a masking of the anode. As a consequence some parts of the anode that are not masked by the covering layer are directly chargeable and residual parts reveal a longer path length to be charged. As the cathode is fully accessible the remaining directly accessible graphite particles are more prone to overcharge like it would be the case at the edges of the anode, if the cathode is larger than the anode. Locally this will be the case according to precision of positioning if anode and cathode are designed equal sized [10]. Comparable findings are shown by Cannarella et al. [11] at the transition of a separator with closed and open pores next to each other. Therefore the described process is assumed to be self-energizing, if a certain amount of covering layer is already present. In the final stage of covering layer evolution in Figure 1d the covering layer becomes compact and impermeable to lithium-ions.

#### Badly connected particles (1C-cell)

For the 1C-cell the half-cell capacities are measured as well (Table 1). However, all values of the anode are below the values of a fresh cell. The DVA shows that anode active material is continuously lost due to full cycling [7]; furthermore it is assumed that the active material is lost locally so that the homogeneity of the cell is reduced. As a result no reliable conclusion of the measured half-cell capacity is possible.

Additionally, insufficient electrically connected particles could cause inhomogeneities. Laser microscope images of fresh cells show already high inhomogeneities. Thus, isolated golden particles are found in a fully discharged fresh cell, which is illustrated in Figure 2a. Furthermore, in a fully charged fresh cell golden particles corresponding to an SOC of about 100% are situated directly next to red colored particles corresponding to an SOC of 60-70 SOC (Figure 2b). As these strongly different SOCs are not compensating each other, the electric connection between the particles and the current collector will be lost or at least very weak. Eventually those particles might be electrically connected and disconnected during

cycling due to volume change of the anode. Assuming that a fully charged particle will be electrically reconnected during the process of charging while the residual electrode is charged until 65% SOC or more. Then, the potential difference of the fully charged particle and the residual electrode is very small in the order of maximum a few mV as the entire anode is situated in the last voltage plateau of the anode. In that case an overcharging of the reconnected particle might occur due to the missing potential difference leading to local plating. If the plated lithium is not completely stripped in the following discharge, at least a fraction of the local plating will become irreversible and passivated by the electrolyte. This process leads to a very slowly increasing inhomogeneity of the charge distribution by the previously described masking due to locally plated lithium. With this, the process of covering layer evolution will start very slowly compared to the first approach of uneven capacity density distribution and the covering layer will grow at very slow pace until the covering layer becomes clearly observable.

This might explain the measurement result of the cell aged at 1C between 45 and 55% SOC exhibiting plating, although the average anode potential is in a safe regime with respect to lithium plating. A region covered with a dense covering layer of one of these cells is highlighted in Figure 2c. In the right laser microscope image no structure of graphite particles but a dense covering layer is recognizable. In the color image several golden (ca. 100% SOC) and silver shining (Li-plating) spots can be observed supporting that theory.

# 3.2 Overcharging of the back side

While the covering layer is developing on primary side of the double-sided coated anode, according to our theory in 3.1, the thickness of the electrode is increasing in the order of µm illustrated in Figure 1 a)-d). As the maximum size of the jelly roll is limited by the cylindrical housing, the distance between anode and cathode at the back side (secondary side) of where the covering layer is forming is decreasing while the separator will be compressed. Therefore, those areas of the back side (secondary side) of the anode will be successively charged faster to higher SOC compared to the residual anode (Figure 1b-e and Figure 3).

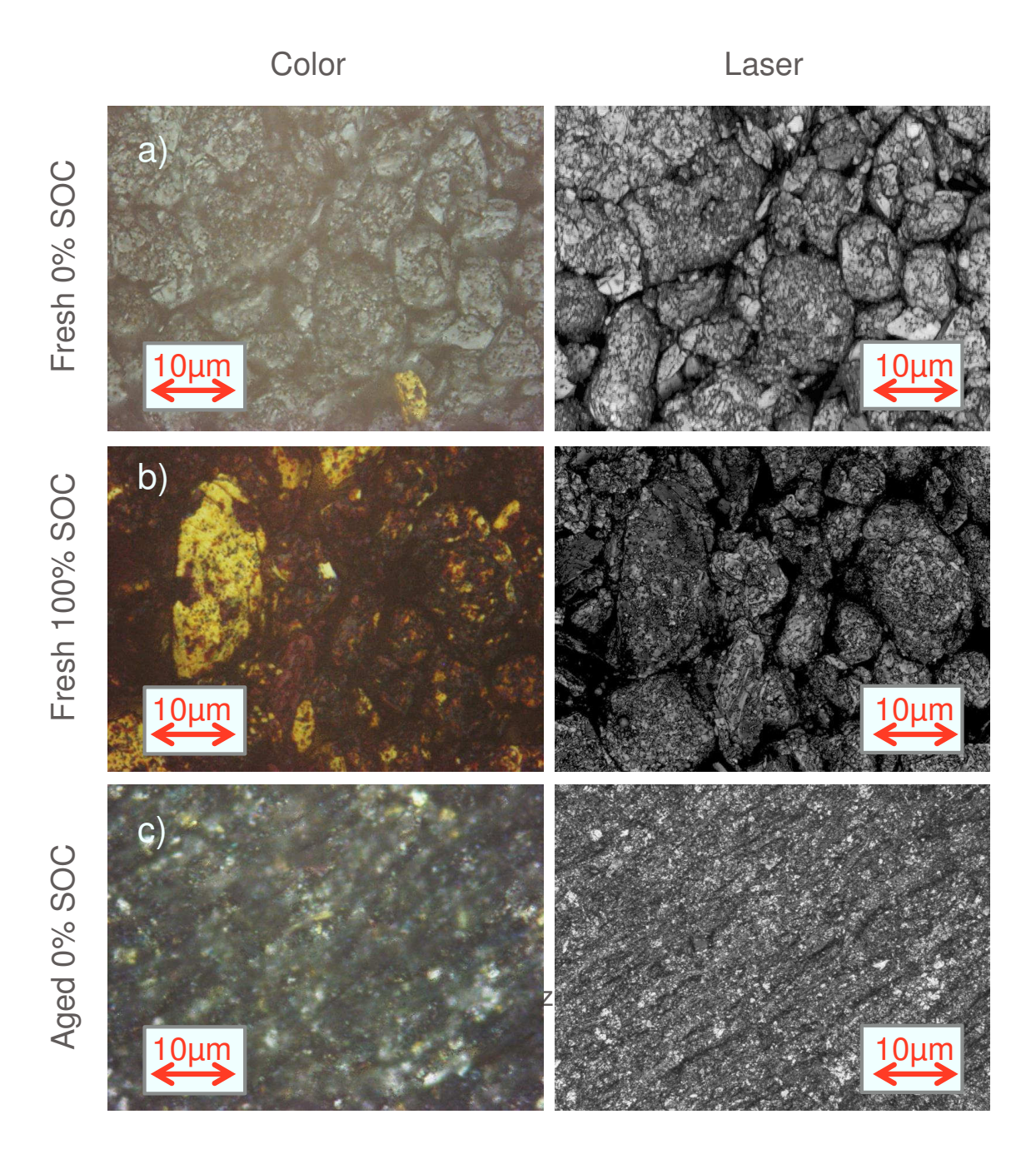


Figure 2 Laser microscope images of a fresh cell at 0% SOC (top), a fresh cell at 100% SOC (middle) and an aged cell at 1C and 10% DOD with dense covering layer (bottom) are shown. All images have the same size while color information is situated on the left and the corresponding the reflectivity can be found on the right.

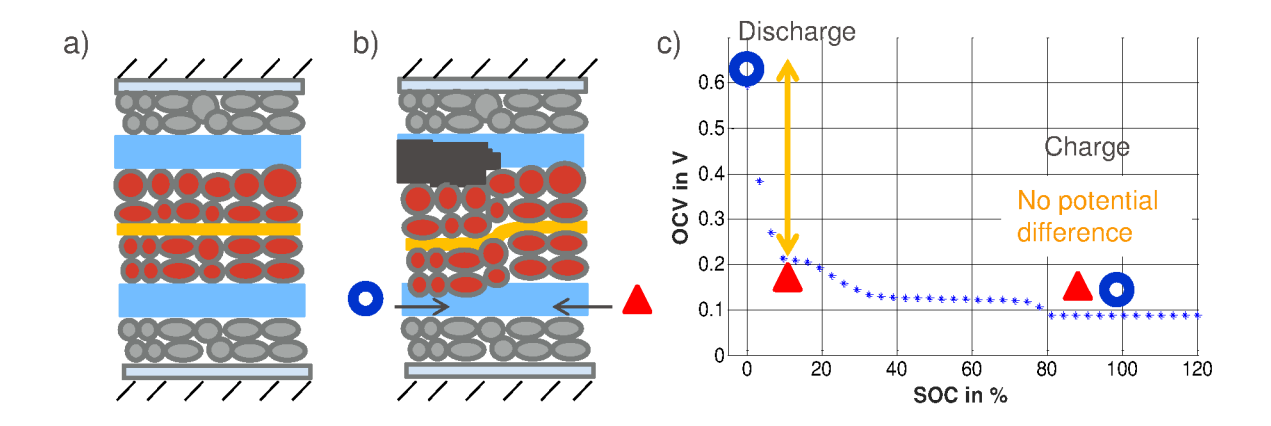


Figure 3 Schematic of the influence of the presence of a µm-thick covering layer on the back side. In a) and b) the anode and cathode stack is limited (by the housing). Is a covering layer present in b), the separator of the back side is compressed and the electrode distance is reduced (marked with ♠) compared to residual parts (marked with ♠). With respect to full cycles the back side of the covering layer ♠ is faster fully charged or discharged. The potential differences between ♠ and ♠ for these two cases at a SOC difference of 10% are described for the anode open circuit curve in c).

The covering layer evolution on the secondary side is supported by an agglomeration effect of active lithium due to lateral flow of active lithium which is illustrated in Figure 3. If during a discharge the better accessible back side of the covering layer marked with ● is already fully discharged and the residual anode marked with ▲ is not fully discharged yet. In that case there is a potential difference between these two anode regions. This potential difference is considerable high as the slope of graphite potential in the delithiated state is very high. It generates a flow of active lithium from the residual anode to the back side of the covering layer. The same process occurs in the reverse direction, if the cell is fully charged. However, in a high lithiation state of the graphite the potential difference is close to zero. This is sketched for an SOC difference of 10% in Figure 3c for fully charge and discharge. As the lithium-ion flow is increasing with increasing potential difference, there is a slow pumping effect at least for high DOD like 100% cycles leading to a lithium-ion agglomeration on the back side of the covering layer. Moreover, the higher SOC at the back side of the anode will increase the thickness due to SOC-dependent volume expansion of the anode and with this

the better accessibility of the back side of the covering layer. The pumping effect will be fastest for nearby residual anode.

If enough remaining active lithium is left, all these findings will support the overcharging of the back side of the primary covering layer. In the end of the process a new covering layer on the back side will be present. However, the influence of inhomogeneous pressure in a full cell is hardly addressed in literature, so that the contribution of each component like the separator, active masses and electrolyte on the parameters diffusion, temperature, electrode distance, active surface and porosity remains vaguely.

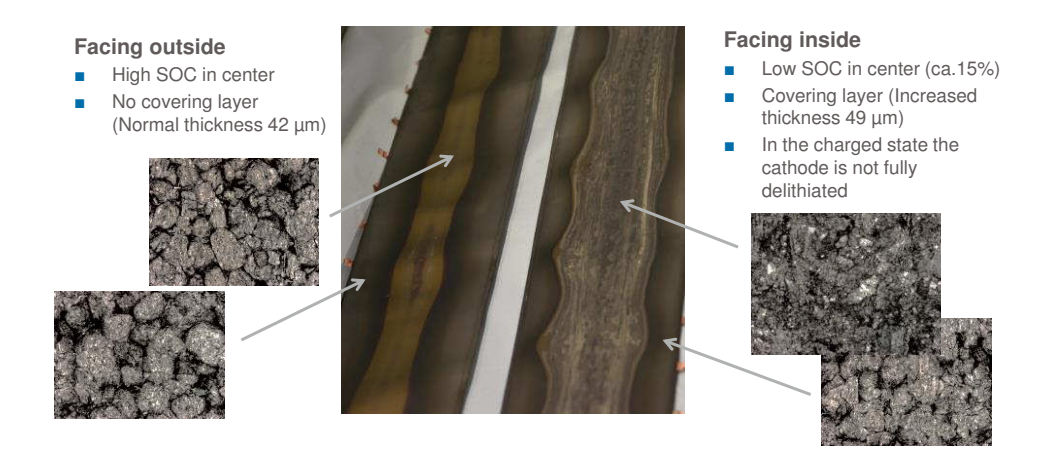


Figure 4 The anode of the 1C-cell disassembled in a fully charged state is displayed. The left part of the image refers to the anode facing to the outside and the right part of the image refers to the back side of the other anode facing inside of the cell. The part facing outside exhibits a highly charged anode in center of about 100% SOC (golden color) while the edges exhibit a comparable low SOC of less than 50% (black colored). In both regions no covering layer is found according to laser microscope images. On the back side (facing inside) a dense covering layer is observable which is eye-catching looking at the laser microscope images.

## 1C-cell

A proof to this theory can be made by looking closer to the 1C-cell aged for 6,500 FCE down to a remaining capacity of 38% (Figure 4). The cell is opened in a fully charged state. On the anode coating side facing outside in direction of the housing a covering layer is observed

while on the anode coating side facing inside the electrode is at least fully charged at a corresponding height position. The thickness of the coating, where the covering layer is found, is increased by 7  $\mu$ m measured with a micrometer screw by comparing the center and the edge parts of the electrode. This increase in thickness due to covering layer corresponds to about 17% of the total thickness of the uncovered anode. Potentially the residual active lithium left in this cell is too low to overcharge the back side of the electrode.

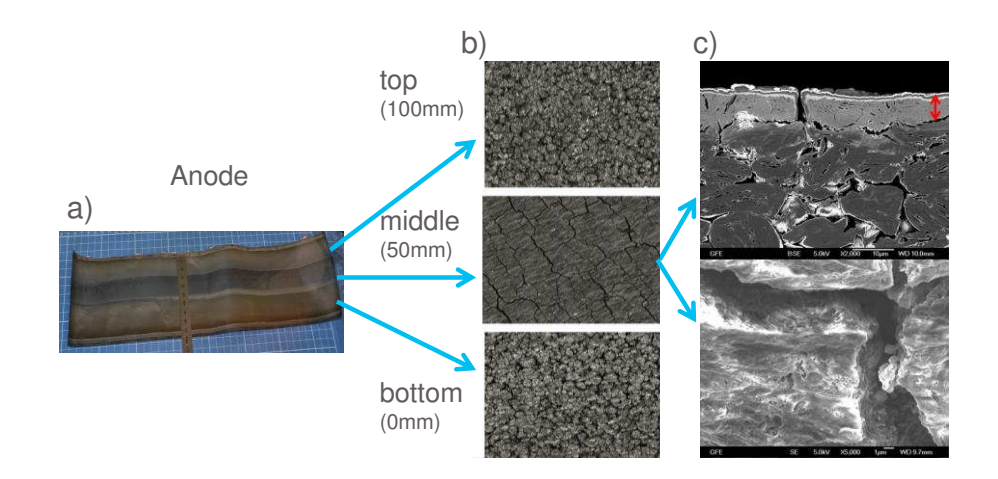


Figure 5 Optical analysis of the cell aged at 2C between 25 and 75% SOC at 40 °C. a) a photography of the anode, b) 3 laser microscope images and c) SEM images (top-cross section, bottom - top view). The cell is disassembled in a fully discharged state and reveals a dense covering layer in the center of both sides of the double-coated anode.

# 2C-cell

What happens, if this process, shown in Figure 4, is completed with enough active lithium, can be observed looking closer to the 2C-cell (Figure 5). A dense covering layer is deposited on the center of the anode on both sides while bottom and top part seems hardly affected (Figure 5b). In Figure 5c top the covering layer can be observed as it is easily distinguishable from the graphite structure. The deposition takes place only on top of the anode facing the separator and cannot be found within the electrode. In Figure 5c bottom the top view on the covering layer shows a dense and fractured layer. Most likely the covering layer breaks apart during unrolling the jelly roll as discussed before for the half-cell capacities. The geometrical

percentage, covered with dense covering layer, is about 30% according to the darker grey of the covering layer visible in the photography in Figure 5a.

# 3.4 Morphology and chemistry of covering layer

In this section the covering layer of the 2C-cell is examined in depth with respect to morphology (mass, density and thickness) and chemistry (EDX and ICP).

## 3.4.1 Thickness and density

The thickness d of the covering layer is up to 9  $\mu$ m measured for the 2C-cell evaluating the cross section image. This is an increase in coating thickness of the anode of about 23% with respect to the thickness of the fresh cell of  $(40\pm1.5)~\mu$ m. The specific mass measured for a fresh cell is  $\rho_{fresh}^{area}=5.8~\frac{mg}{cm^2}$ . For the aged cell at the location of the covering layer the specific mass is  $\rho_{center}^{area}=6.6~\frac{mg}{cm^2}$  and at the normal aged parts at the bottom and top it is  $\rho_{top/bottom}^{area}=6.0~\frac{mg}{cm^2}$ . The areal density of the covering layer is  $\rho_{CL}^{area}=\rho_{center}^{area}-\rho_{fresh}^{area}=0.8~mg/cm^2$ . Assuming a homogenous mass distribution over the electrode, the density of the covering layer can be calculated by:

$$\rho_{CL}^{volume} = \frac{\rho_{CL}^{area}}{d}$$
 (1)

to 0.89  $\frac{g}{cm^3}$ .

#### 3.4.2 SEM and EDX

The SEM and EDX measurements of the 2C-cell are given in Figure 6. The preparation is done by Ar-milling to realize a homogeneous cross section. Ar-milling is performed under normal atmosphere. Unfortunately the particular X-ray detector on this SEM cannot detect Li due to low energy resolution of standard EDX. Due to the lack of outer shell electrons H is also not detectable as characteristic X-ray peaks are missing. The spectra of the graphite parts labeled as 4-7 in lower part of the SEM micrograph return a high amount of C, originated from the graphite active material, Carbon black, as a conductive additive, and solvents of the electrolyte. Furthermore, a slight amount of F and P are measured that can

be associated to the conductive salt  $LiPF_6$  or a decomposition product in the form of dried electrolyte or as component in the SEI respectively. The O-peak is likely caused by electrolyte residues or by reaction with air during the cell preparation.

In contrast, the covering layer labeled as 1-3 exhibits less C but reasonable amounts of O, P, F, Fe and S. The C peak will be originated mainly from the graphite, but might also have contributions from residues of the carbonate solvents. P and F can be assigned to the conductive salt and Fe from dissolution from the cathode active material. The presence of S could be measured in ICP measurements of fresh cells as well and might result from impurities of the active materials. Summing up the covering layer contains Fe, S and residues of the solvents and the salt ( $LiPF_6$ ) of the electrolyte.

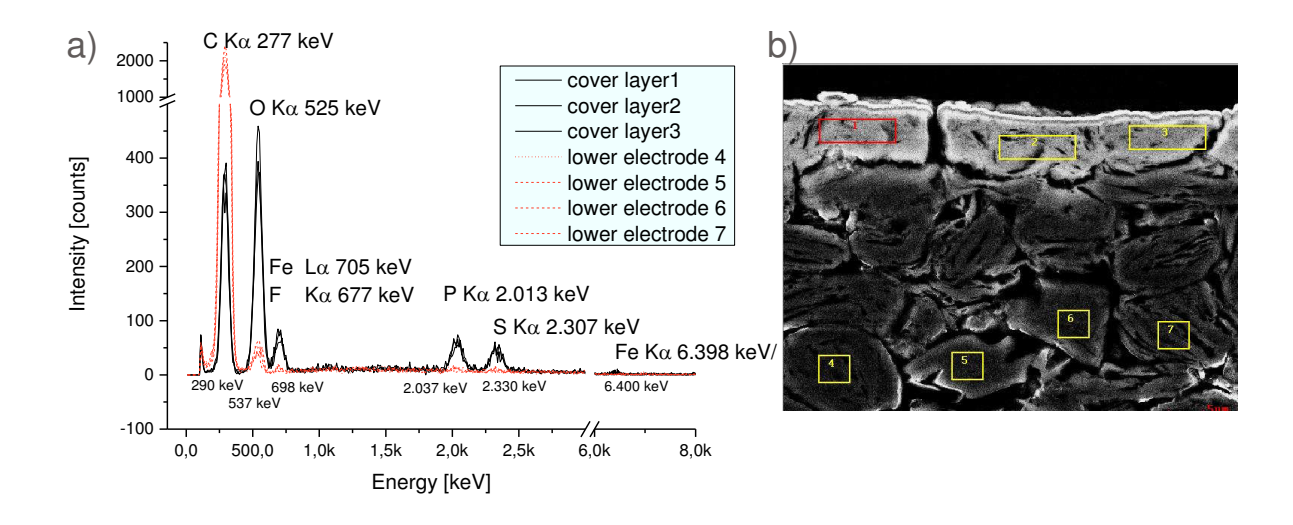


Figure 6 EDX-Spectra (a) of the corresponding areas highlighted in the SEM picture (b).

#### 3.4.3 ICP

As an alternative element identification and quantification method ICP measurements are evaluated for the 2C-cell. The content of the elements H, O and C are unfortunately not soluble in aqua regia or not measureable with ICP. ICP results of the electrode height revealing a compact covering layer ( $\rho_{center}^{area}$ ) are related on one hand to the top and bottom parts ( $\rho_{top/bottom}^{area}$ ) that do not show any covering layer and on the other hand to the fresh cell ( $\rho_{fresh}^{area}$ ). By correlating the results on one side to the fresh cell and on the other to the

top/bottom part an over- and underestimation is obtained. The difference is assigned to  $\Delta \rho_{CL}^{area}$ .  $\Delta \rho_{CL}^{area}$  is calculated with respect to the difference to the areal density of the covering layer  $\rho_{CL}^{area}$  =0.8 mg/cm² calculated before. The results are summarized in Table 2.

21-34% of the mass of the covering layer could be linked to measurable elements. The rest mass might consist of F and residues of electrolyte (C, H and O). Using the density of lithium metal of  $0.53 \frac{g}{cm^3}$  the volumetric lithium share of the covering layer is 23-40%.

Table 2 Spatial-resolved ICP results of the anode. The fresh cell is related to non-covered part  $(\rho_{top/bottom}^{area})$  and the covered parts  $(\rho_{center}^{area})$ .  $\Delta\rho_{CL}^{area}$  represents the span of the difference to the non-covered and fresh electrode. The ratio of  $\Delta\rho_{CL}^{area}$  of the specific element to the total density of covering layer  $\rho_{CL}^{area}=0.8\,\frac{mg}{cm^3}$  is marked as  $\frac{\Delta\rho_{CL}^{area}}{\rho_{CL}^{area}}$ . All values are given in  $\frac{mg}{cm^2}$ 

Element	$ ho_{fresh}^{area}$	$ ho_{top/bottom}^{area}$	$ ho_{center}^{area}$	$\Delta ho_{CL}^{area}$	$rac{\Delta ho_{CL}^{area}}{ ho_{CL}^{area}}$
Lithium	0.13	0.21	0.32	0.11-0.19	14-24%
Phosphorus	0.06	0.06	0.06	0.00	0%
Sulfur	0.02	0.04	0.07	0.03-0.05	4-6%
Iron	0-0.01	0.01	0.03	0.02-0.03	3-4%
Sum				0.16-0.27	21-34%

#### 3.4.4 Discussion

To sum up a high fraction of the covering layer of 23-40% with respect to volume consists of pure lithium (ICP). A high percentage of the residual volume will consist of the electrolyte components H, C and O as the other elements are found only in low quantities in ICP and EDX. Furthermore, the density analysis is supporting this theory. The volumetric densities of the elements, salts and solvents that are expected in this specific cell are summarized in Table 3. The calculated density  $0.89 \, \frac{mg}{cm^3}$  of the covering layer is not well described with solely lithium-metal with a density of  $0.53 \, \frac{mg}{cm^3}$  and very low quantities of heavier elements.

Thus, the residual elements should exhibit a slightly higher density than  $0.89 \ \frac{mg}{cm^3}$  which is the case for the densities of the non-aged electrolyte components summarized in Table 3. As P and F are found in the covering layer in EDX, it is very likely that LiPF<sub>6</sub> is bound within the covering layer. The missing lateral concentration differences of P measured with ICP leads to the assumption that only LiPF<sub>6</sub> at a specific lateral position is bound or decomposed in covering layer and no significant lateral transport of LiPF<sub>6</sub> occurs. Therefore, the findings of the density analysis, ICP and the EDX measurements support the theory of slow growing covering layer caused by lithium plating passivated by the electrolyte.

Table 3 Densities of all elements [12], salts and solvents [13] found in the covering layer according to EDX and ICP measurements and in the electrolyte.

Elements/	Mass density
Solvents	$ \ln \frac{g}{cm^3} $
Li	0.53
Fe	7.86
S	2.07
0	1.43
С	3.51
LiPF <sub>6</sub>	1.5
DMC	1.07
EC	1.32
EMC	1.01
DEC	0.97

According to ICP the values of S and Fe are increased, if the covering layer is present. The presence of Fe was found for this cell type for storage tests at 60 °C and is increasing with storage SOC as written in our previous publication [2]. By evaluating the floating current for calendaric aging at 100% SOC of the same cell type [14], a different aging mechanism could be identified from 50 °C on, which likely will be linked to Fe dissolution. Moreover the Fe deposition is shown by Li et al. [15] on the surface of the anode measured with Raman and XPS. In our previous publication the DVA evaluation of these cells [7] shows that the Fe

deposition could be associated to clog pores of the graphite active material, which is in accordance to Li et al. [15]. This would lead to a masking of the anode surface which accelerates the covering layer evolution as described before. Thus, local high temperatures of more than 50 °C induced by cycling might cause the increase of Fe. Whether the Fe dissolution is causing the covering layer or is caused by the accompanied conditions of the covering layer evolution cannot be clarified in this work. The role of S according to the development of covering layer or potential catalytic effects accelerating the aging is not clear to the authors, too.

## 3.5 Deactivation of electrode

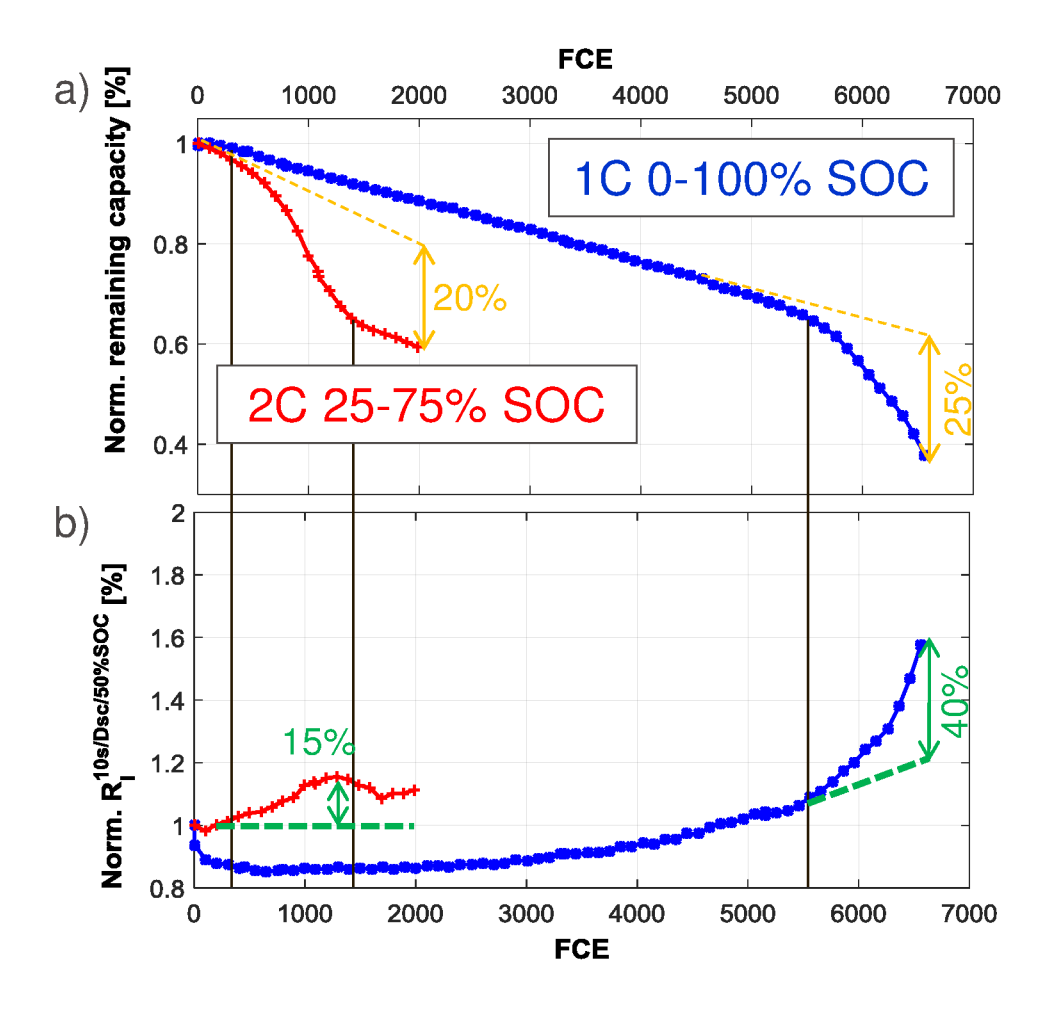


Figure 7 a) The trend over aging of the capacity fade and b) rise of internal resistance is illustrated for the 1C-cell and the 2C-cell. Slope changes indicate covering layer evolution.

## 3.5.1 Extractable capacity

A compact layer on top of the anode as shown in Figure 6 is impermeable to lithium-ions or to the dissolved conductive salt respectively. Therefore, such a compact layer will lead to a deactivation of the covered anode and their opposed cathode due to the increased diffusion length of the lithium-ions during charging and discharging. These parts of the anode and cathode will be called *passive anode* and *passive cathode*. If some active lithium is stored in the passive anode or passive cathode while the covering layer becomes compact, this active lithium is lost for normal operation like capacity tests. However, this capacity could be extracted for very low discharge rates regarding low potential of the anode at the end-of-discharge leading to a lithium-ion flow from the passive anode to the active part (passive electrode effect described in [2]). As the potential curve of the LiFePO<sub>4</sub> cathode is very flat and exhibits a reasonable potential difference only at the fully charged state nearly no compensation lithium-ion currents between the active and passive cathode is assumed between 0-94% SOC.

Summing up, the loss of active lithium during cycling is amplified in the moment the covering layer becomes impermeable and the active lithium that is stored in the emerging passive anode and cathode is not extractable anymore. Therefore, the slope of capacity fade is increasing in this period of evolution of the covering layer as the continuous linear-like loss of active lithium is superposed by active lithium trapped in anode and cathode behind the covering layer. If the formation of covering layer is concluded, the slope of the capacity loss will become the same as before the formation of covering layer: This is only valid if there is a low influence on the increasing actual C-rate as the capacity and active area are reduced. This also implies that, if a deposition would not lead to a closed compact layer, but to an open pore deposition, no acceleration of the slope of the capacity fade would be expected.

In Figure 7a the expected change in slope of the capacity fade is visible for the 1C-cell and the 2C-cell. The slope changes are indicated by vertical lines. For the 2C-cell the slope of the aging reduces to even moderate values before end of test. Thus, for the 2C-cell the covering

layer is completed and compact covering layers on both sides of the anode are formed, while for the 1C-cell the process of covering layer evolution is not yet completed on both sides. These results perfectly agree to the PMA results given in the previous sections 3.1 and 3.2.

One major difference between those two cells is that the covering layer for the 2C-cell starts almost immediately after begin of test while the 1C-cell is aged more than 5,000 FCE down to 65% remaining capacity before the slope increase is observable. Again this is matching to the previous post-mortem results as the faster aging 2C-cell suffers from inhomogeneous coating. With this, the 2C-cell already contained enough inhomogeneities (described in section 3.1) to form the covering layer directly, while for the 1C-cell the inhomogeneities needed to be successively increased before the process of covering layer evolution started.

## 3.5.2 Active lithium within passive cathode

As discussed before the slope change is not caused by the simple deactivation of cathode and anode but by the trapped active lithium in the passive electrodes that are not available for cycling. This theory will be supported by ICP measurements.

#### Fresh cell

All fresh cells with 0% SOC reveal  $\frac{Li_c}{Fe_c}$  (100% SOC)= 81% of lithium normalized to Fe on cathode with respect stoichiometry. 13% points of the residual 19% of lithium is found within the anode and the residual 6% are not directly measurable on the anode and supposed to be found within the overhang of the anode. This matches to the fact that the SOC is 99% before the test and the share of overhang to an active electrode is 5.9% [2]. Or in other words the overhang is fully charged with about 6% of the active lithium missing in the active part of the cell.

Disassembling a fresh cell at 100% SOC, a lithium content of  $\operatorname{Li}_c^{\operatorname{Fe}_C}(0\% SOC)=6\%$  on the cathode is measured. Therefore,  $\frac{Li}{Fe_C}(active)=75\%$  refers to 100% extractable capacity. In that case all active lithium is situated on the anode and adds up to the passivated lithium.

The expected value for a disassembled cell at 0% SOC is calculated with the actual capacity  $C_{\rm actual}$ :

$$\frac{Li_C}{Fe_C} = \frac{C_{\text{actual}}}{C_0} \cdot 75\% + 6\% \qquad (2)$$

#### 2C-cell

The 2C-cell is disassembled at 0% SOC. Therefore, in ICP measurement the active lithium should be found solely in the cathode and all passivated lithium should be found on the anode side. This is in good agreement to half-cell measurements of the anode vs. metallic lithium where no active lithium is extractable during the first charge from the graphite anode. Nota bene, the anode capacity is fully accessible as the compact covering layer breaks after unrolling the jelly roll, which can be seen in Figure 5. Hence, all active lithium of the deactivated electrodes should be found on the cathode side. The ICP results for the 2C-cell are given in Table 4. On the cathode 13% points more active lithium is measured than it would be expected according to loss of full cell capacity of  $\frac{Li_C}{Fe_C}$  (expected) = 50%.

The actual value is  $\frac{Li_C}{Fe_C}(measured)$  =63% which corresponds according to Equation (2) to:

$$\frac{C_{\text{actual}}}{C_0} = \frac{\frac{Li_C}{Fe_C} (measured) - 6\%}{75\%} = 76\% \pm 3\% \quad (3)$$

The uncertainty originates from the ICP measurement technique for absolute quantities which is in the order of  $\pm 3\%$ . The deviation in capacity loss derived from the ICP measurements  $\frac{C_{actual}}{C_0}$  and measured by capacity tests is 76%-59%=17%. The value of 17% deviation correlates quite well to the capacity deviation during the phase of higher slope of capacity loss of about 20% indicated in orange in Figure 7a. The slightly lower values will originate from higher formation losses before begin of test due to the high spread of specific anode capacity as discussed before.

Table 4 Comparison of the expected values, according to remaining capacity  $\frac{C_{actual}}{C_0}$  to the results of the ICP measurement of the lithium content of the cathodes of the 2C-cell  $\frac{Li_C}{Fe_C}$  at the end of test after 2,000 FCE. The measurement data is averaged out of 15 measurement points that are distributed over length and height of the electrode. The cell is disassembled at 0% SOC.

Disassembled	Fresh	2C-cell cathode	
at 0% SOC	cathode		
		Expected	Measured
$\frac{C_{actual}}{C_{0}}$	100%	59%	59%
Li <sub>C</sub> Fe <sub>C</sub>	81%	50%	63%

In the following approach the additional slope change is correlated to the covered area. The active lithium of covered anode and opposed cathode is not usable for charging and discharging as the covering layer is non-permeable to lithium-ions. The area of deactivated electrode of the 2C-cell is according to the photography in Figure 5a about 30% of the total area. The electrode can be separated into the top-bottom part and the center part (covering layer in Figure 5b). This is sketched in Figure 8. The local SOC is calculated with the active lithium at begin of test of  $\frac{Li_C}{Fe_C}$  (t=0) = 75% and non-extractable lithium  $\frac{Li_C}{Fe_C}$  =6% within the cathode:

$$SOC_{local} = \frac{\frac{Li_C}{Fe_C} - 6\%}{\frac{Li_C}{Fe_C} (t = 0)}$$
 (4)

As the lithium in the center is not participating, the actual capacity is solely calculated by the top and bottom part multiplied to the area:

$$C_{actual}^{calc} = SOC_{local}^{top/bottom} \cdot area_{local}^{top/bottom}$$
 (5)

Table 5 Calculating the loss of capacity evaluating ICP measurements of the lithium found on cathode according to Equation (4) and the percentage of the covered area in the electrode's center applying Equation (5).

	Top/bottom	Center
$\frac{Li_C}{Fe_C}$	70%	54%
SOC <sub>local</sub>	85%	65%
Area	70%	30%
C <sub>actual</sub>	60%	0%

All results are summarized in Table 5. The simple calculation results in an actual capacity of 60% which is very close to the measured extractable capacity of 59%. Thus, the two demonstrated strategies to explain the deactivated lithium on the cathode via average lithium content of 15 positions on the cathode and via 30% deactivated part in the center return the same results and support the theory of a regional well-defined covering layer that is impermeable to lithium-ions.

Table 6 Comparison of the expected values, according to remaining capacity  $\frac{C_{actual}}{C_0}$  to the results of the ICP measurement of the lithium content of the cathodes  $\frac{Li_C}{Fe_C}$  of the 1C-cell at the end of test after 6,500 FCE. The measurement data is averaged out of 15 measurement points distributed over length and height of the electrode. The cell is disassembled at 0% SOC.

Disassembled	Fresh	1C-cell cathode	
at 100% SOC	cathode		
		Expected	Measured
$\frac{C_{actual}}{C_0}$	100%	38%	38%
Li <sub>c</sub> <sup>Fe</sup> c	6%	6%	28%

In the PhD thesis of Johannes Schmalstieg [16] the effect of a dense covering layer on capacity fade could be simulated with a good accuracy using the given theory.

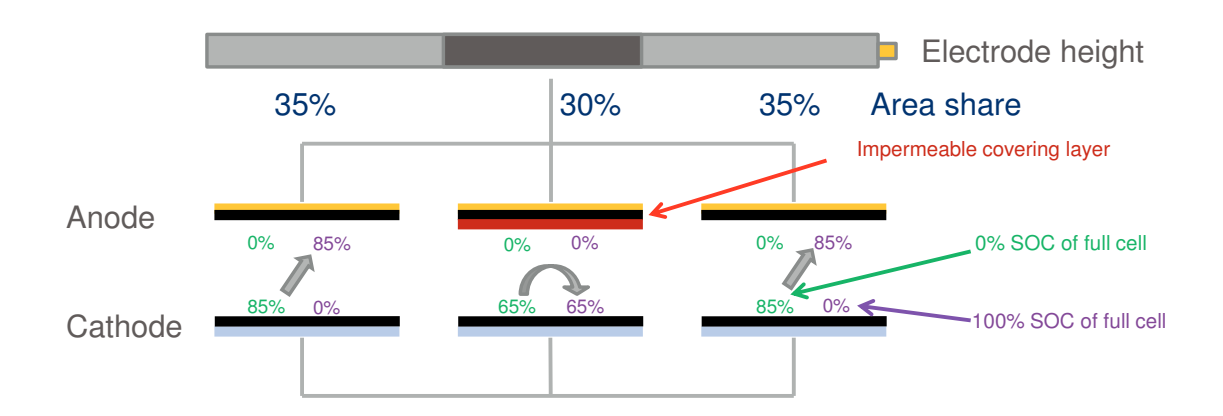


Figure 8 In this representation the 2C-cell is virtually divided into three parallel connected parts that are either deactivated by a passivation layer (center, red) or behave like a fresh cell (right and left). In the top the percentage of the corresponding area is stated. Between anode and cathode the distribution of the active lithium according to ICP for each part is given for the charged and discharged state of the full cell. The values  $SOC_{local}$  for the discharged state of the full cell (green) are calculated according to Table 5 and Equation (4). For the fully charged state of the full cell the assumption is made that no charge transfer takes place and all active lithium remains within the cathode.

## 1C-cell

The 1C-cell is disassembled at 100% SOC and the results are given in Table 6. The deviation between the expected and the measured value of  $\frac{Li_C}{Fe_C}$  is 22% points which corresponds to an additional capacity loss of  $\frac{22\%}{75\%} = 29\% \pm 3\%$ . Again this is in the order of magnitude of the value of 25% for the additional capacity loss obtained graphically in Figure 7. Deviations will result from the challenge to represent inhomogeneous lithium distribution with limited measurement points. The inhomogeneous distribution of active lithium visible in Figure 4 resulting from non-uniform boundary conditions discussed before, eventually will lead to reach cut-off voltages earlier. This is supported by the fact that in a calculation over

the deactivated area only 60% would be sufficient to explain 25% additional losses of the increasing slope of capacity fade.

## 3.5.3 Internal resistance with pulse tests

#### 2C-cell

In the case the passive electrodes would not contribute to a 10 s pulse and 30% of the anode is passive due to a dense covering layer the internal resistance should be increased to  $0.7^{-1}$  x 100% = 143% of its initial value. According to the measurement the internal resistance just rises up to 115% for the 2C-cell (Figure 7b). However, this can be explained by looking closer to the absolute values of the internal resistance. The absolute internal resistance of the 2C-cell at begin of test is  $8.55 \text{ m}\Omega$ ; towards end of test it varies in the corridor of  $R_i^{EOT} = 9.51 - 9.88 \text{ m}\Omega$ . Calculating back from the final values, the expected initial values are calculated by  $R_i^{BOT} = R_i^{EOT} \cdot (143\%)^{-1}$  to 6.65- $6.91 \text{ m}\Omega$ . This matches very good to the  $R_i^{BOT}$  of all other cells in this tests which are between  $6.5 \text{ m}\Omega$ . and  $7.5 \text{ m}\Omega$ . Thus probably due to the inhomogeneous coating of the graphite anode as reported before the SEI is formed nonhomogeneously which induced already an increase of internal resistance during formation before starting the tests.

### 1C-cell

With respect to the 1C-cell until 5,500 FCE the rise of internal resistance follows the trend of cells aged under the same test condition until minimum 4,000 FCE as the test for the two other cells were stopped [2]. All cells revealed a linear capacity fade until 4,000 FCE. The stronger increase of the slope of the internal resistance is calculated from 5,000 FCE on.

The reasons for the initial decrease of the internal resistance of more than 10% can only be vaguely estimated. Maybe this is caused by a homogenization effect during full cycling due to high voltage slopes and the end of charge and discharge as it was discussed for DVA [7]. Inhomogeneously loss of anode active material will be most likely the reason for the smooth increase of internal resistance until 5,500 FCE due to the performed full cycles leading to

many high volume changes especially on the anode. This is supported by DVA where the distance of the characteristic minima of the anode is reduced. The detailed DVA evaluation including half-cell tests is published here [7].

The initial absolute internal resistance is measured to 6.795 m $\Omega$ , so that a reasonable aging before begin of test can be excluded. The calculation of the increase of internal resistance is not as easy to calculate as for the 2C-cell, because of the not yet fully defined evolution of the covering layer and the not equally distributed active lithium in the uncovered active anode. The additional increase of the internal resistance during covering layer evolution according to the graphical approach in Figure 7b is estimated to about 40% points. With respect to Figure 4 the covered area facing outside is zero and facing inside it is about (55±5)%. Thus, in total about 25-30% of the entire anode area is covered, so that the remaining area only contributes to the pulse test which leads to an increase of internal resistance of 133-143%. The results fit quite well to the increased internal resistance of 40% points. Furthermore the back side is highly charged in the cell's center while the residual anode exhibits a significantly lower SOC which might contribute to the internal resistance, too.

# 4. Conclusions

The dense covering layer that is observable for certain cyclic aged cells was characterized in this contribution. It is likely formed by slow lithium plating as 23-40% of the volume of the covering layer consists of lithium (EDX, ICP and density) and needle-like structures are observable in early stages of the formation of covering layer. The residual part of the covering layer consists of electrolyte residues as it is found for SEI formation and deposited Fe and S. While the influence of S is not clear yet, the Fe dissolution is associated to temperatures higher than 50 °C which might be fulfilled locally considering resistive heat generation.

The covering layer might be primarily generated out of two primary reasons. One reason is an inhomogeneous specific capacity distribution due to bad coating leading to a fast evolution of a covering layer. The other reason is the overcharging of isolated badly electrically connected particles leading to a comparable slow evolution of a covering layer. Even the deposition of Fe could enhance the covering layer evolution due to masking of the anode surface of the covering layer. The masking of the covering layer generally accelerates the formation of covering layer.

As the covering layer leads to an increasing thickness of the anode, the back side of the covering layer is better connected to the cathode as the electrode distance is reduced on behalf of the separator due to increased pressure. Therefore, the back side of the covering layer will be discharged faster to 0% and charged faster to 100% SOC. The potential difference on anode between the better accessible and the residual part is higher discharging to 0% SOC compared to charging to 100% SOC. With this, if full cycles are applied, lithium is slowly pumped, due to the passive electrode effect, from the residual anode towards the better accessible part of the anode at the back side of the covering layer.

If the covering layer becomes compact, no lithium-ions may pass through the covering layer.

Therefore, those parts of the anode and the opposed cathode are successively deactivated

with respect to capacity and internal resistance. This was successfully proved by correlating the slope change of capacity and internal resistance trends of two cells with the percentage of the covered anode area. Furthermore ICP measurements of the cathode exhibit higher amounts of active lithium than it was expected by loss of capacity.

# **Acknowledgement**

The results are generated during the project MEET-HiEnD (03X4634B). We like to thank the Bundesministerium für Bildung und Forschung (BMBF) for funding and Johan Persson from the Gemeinschaftslabor für Elektronenmikroskopie (GFE) for the SEM and EDX support. Special thanks are dedicated to Stefan Käbitz and Johannes Schmalstieg for their scientific inspiration, Jens Münnix for his active support in post-mortem-analyses and Rita Graff for her support and ideas in analytics.

# Literature

- [1] M. Kassem, C. Delacourt, Postmortem analysis of calendar-aged graphite/LiFePO4 cells, J. Power Sources. 235 (2013) 159–171. doi:10.1016/j.jpowsour.2013.01.147.
- [2] M. Lewerenz, J. Münnix, J. Schmalstieg, S. Käbitz, M. Knips, D.U. Sauer, Systematic aging of commercial LiFePO4jGraphite cylindrical cells including a theory explaining rise of capacity during aging, J. Power Sources. 345 (2017) 254–263. doi:10.1016/j.jpowsour.2017.01.133.
- [3] M. Lewerenz, A. Warnecke, D.U. Sauer, Introduction of capacity difference analysis (CDA) for analyzing lateral lithium-ion flow to determine the state of covering layer evolution, J. Power Sources. 354. (2017) 157–166.

  doi:10.1016/j.jpowsour.2017.04.043.
- [4] M. Klett, R. Eriksson, J. Groot, P. Svens, K. Ciosek Högström, R.W. Lindström, H. Berg, T. Gustafson, G. Lindbergh, K. Edström, Non-uniform aging of cycled commercial LiFePO4//graphite cylindrical cells revealed by post-mortem analysis, J.

- Power Sources. 257 (2014) 126-137. doi:10.1016/j.jpowsour.2014.01.105.
- [5] M. Klett, P. Svens, C. Tengstedt, A. Seyeux, S. Jolanta, G. Lindbergh, R. Wreland, Uneven Film Formation across Depth of Porous Graphite Electrodes in Cycled Commercial Li-Ion Batteries, J. Phys. Chem. C. 119 (2015) 90–10. doi:10.1021/jp509665e.
- [6] B. Stiaszny, J.C. Ziegler, E.E. Krauß, J.P. Schmidt, E. Ivers-tiffée, Electrochemical characterization and post-mortem analysis of aged

  LiMn2O4eLi(Ni0.5Mn0.3Co0.2)O2/graphite lithium ion batteries. Part I: Cycle aging, J. Power Sources. 251 (2014) 439–450. doi:10.1016/j.jpowsour.2013.11.080.
- [7] M. Lewerenz, A. Marongiu, A. Warnecke, D.-U. Sauer, Differential voltage analysis as a tool for analyzing inhomogeneous aging: a case study for LiFePO4|Graphite cylindrical cells, J.Power Sources. 368 (2017) 57–67.

  doi:https://doi.org/10.1016/j.jpowsour.2017.09.059.
- [8] W. Lu, C.M. López, N. Liu, J.T. Vaughey, A. Jansen, D.W. Dees, Overcharge Effect on Morphology and Structure of Carbon Electrodes for Lithium-Ion Batteries, J. Electrochem. Soc. 159 (2012) A566. doi:10.1149/2.jes035205.
- [9] M. Petzl, M. Kasper, M.A. Danzer, Lithium plating in a commercial lithium-ion battery -A low-temperature aging study, J. Power Sources. 275 (2015) 799–807. doi:10.1016/j.jpowsour.2014.11.065.
- [10] K. Eberman, P. Gomadam, G. Jain, E. Scott, Material and Design Options for Avoiding Lithium Plating during Charging, ECS Trans. . 25 (2010) 47–58. doi:10.1149/1.3414003.
- [11] J. Cannarella, C.B. Arnold, The Effects of Defects on Localized Plating in Lithium-Ion Batteries, J. Electrochem. Soc. 162 (2015) A1365–A1373. doi:10.1149/2.1051507jes.
- [12] https://www.webelements.com, (n.d.). https://www.webelements.com.

- [13] Gefahrstoffdatenbank (GESTIS), (n.d.). http://www.dguv.de/ifa/gestis/gestis-stoffdatenbank/index.jsp.
- [14] M. Lewerenz, J. Münnix, J. Schmalstieg, S. Käbitz, M. Knips, A. Warnecke, D.U. Sauer, New method evaluating currents keeping the voltage constant for fast and high resolved measurement of Arrhenius relation and capacity fade, J. Power Sources. 353 (2017) 144–151. doi:10.1016/j.jpowsour.2017.03.136.
- [15] D. Li, D.L. Danilov, L. Gao, Y. Yang, P.H.L. Notten, Degradation Mechanisms of the Graphite Electrode in C 6 /LiFePO 4 Batteries Unraveled by a Non-Destructive Approach, J. Electrochem. Soc. 163 (2016) A3016–A3021. doi:10.1149/2.0821614jes.
- [16] J. Schmalstieg, Physikalisch-elektrochemische Simulation von Lithium-Ionen-Batterien-Implementierung, Parametrierung und Anwendung, RWTH Aachen University, 2017.